Development of Elastomeric Rubber Bearing Utilizing Core-and-Filler System

Kar Chun Tan[a], Farzad Hejazi[a,*], Hojjat Mohammadi Esfahani[a] and Thomas Chong[b]
[a] *Department of Civil Engineering, University Putra Malaysia, 43400,Selangor,Malaysia*
[b] Hercules Engineering (SEA) Sdn bhd, Sungai Buloh, Malaysia
* Corresponding author. Email: farzad@fhejazi.com

Abstract
Elastomeric bearing is the most common base isolation system for structures and bridges to dissipate effect of applied vibration and ground motion. To improve performance of the base isolators, lead core is implemented in the rubber bearings and it successfully enhances the damping and stiffness of elastomeric bearing.
However, the most notable disadvantage of lead-core rubber bearing is the lead toxicity impact on extensive environmental contamination, which restrained application of lead in construction industry.
Therefore, in the present study, an attempt has been made to develop a new elastomeric laminated bearing utilizing core-and-filler system instead of lead core to improve the performance of bearing. Two types of filler, namely granular and shape memory polymer are implemented. Granular filler is prepared by using silica sand, while shape memory polymer filler is prepared by using epoxy resin. Also, steel core is implemented to improve the stiffness of filler.
The performance of proposed bearing utilizing with core-and-filler system is evaluated using finite element simulation. The numerical results revealed the efficiency of bearing with proposed system by providing considerable damping and stiffness. The replacement of lead core with fully filled granular and shape memory polymer showed improvement in terms of stiffness, and this proved core-and-filler system is effective in limiting lateral displacement.
Also, the prototype of base isolation devices with both granular and shape memory polymer fillers are fabricated and tested via cyclic shear test. The results are compared with finite element analysis results, and good agreement between experimental tests results and numerical simulation response is shown. The experimental testing results proved that implementation of core-and-filler system improves the lateral resistance of proposed elastomeric bearing. In overall, it can be concluded that the implementation of core-and-filler system provides a reliable improvement to the performance of conventional elastomeric bearing and can be considered as alternative system to lead core rubber bearings.
Keywords: Elastomeric isolator, laminated rubber bearing, lead core rubber bearing, core and filler system, sand, epoxy resin, finite element method

1.0 Introduction

Base isolation technology has been a matured energy dissipation technology in recent years. Laminated rubber bearing (LRB) is one of the simplest and most economical devices for the purpose [1][2]. Alternating layers of steel plates and rubber sheets in this device dissipates energy from ground motion before it can be transmitted to superstructure [3]. The device reduces the fundamental frequency of superstructure and thus makes it stay out of the range of ground motion frequencies that contains principal energy [4][5][6].
The performance of LRB can be improved by introducing lead core. Studies have proved that the resulted lead core rubber bearing (LCRB) shows significant shear and compression stiffnesses compared to LRB. Moreover, by exploiting the property of lead that yield under considerably low stress of 10MPa and recrystallizes in room temperature, the damping property of bearing is highly improved while being consistent [6].

Another alternative to LRB, fibre-reinforced rubber bearing (FRRB) that uses fibre reinforcement material (FRP) instead of reinforcing steel plates is used. The substitution directly reduces the weight and manufacturing cost of the device, compared to LRB. It is also proven from study that, the friction between FRP and rubber can improve the bearing's damping and energy dissipation capacity, as well as compression stiffness [8][9].

Among the discussed variation of bearing devices, LRB and LCRB are commonly used in the construction industry. However, major drawbacks from the application have been an issue. In practice, an elastomeric bearing is designed to deform by an allowable magnitude when subjected to forces as specified in codes and standards. In the event of unforeseen situations, forces that act on superstructure may cause the bearing to deform unexpectedly. Such change prompts the bearing to respond with large strain, and this causes the hardening of rubber and loses its flexibility. As a result, less force will be filtered by the isolator and being transferred to superstructure, causing the structure to sustain significant force and acceleration [8][10]. On the other hand, when the bearing does not work as intended, uncontrollably large deformation can happen and resulting in unseating failure. The superstructure may not be stable and at the risk of collapse or topple over [11].

The use of lead in bearing technology on the other hand, brings harm alongside improvement. It has been proven that lead contaminates soil, and its effect can persist for centuries [12][13]. People reside in or nearby these areas are at high risk of lead exposure, and such exposure always bring adverse impact to human health [14][15].

Several studies were conducted to innovate the elastomeric bearing technology. Matsushita, Fujisaka and Sasaki proposed peripherally restrained bearing (PRB). The PRB is similar to LRB, with the only key difference where the centre of the bearing is filled with synthetic rubber block, namely core block. Due to this configuration, the alternating rubber layers and steel plates are forming restraining rings that help to restrain the homogeneous core block from bulging. The damping of the core block used is greater than the rubber in peripheral restraining ring, result in greater damping ratio of the PRB device compared to LRB. The test result also revealed that the critical shear strain of PRB is lower than that of LRB, and the researchers remarked that the deficiency has insignificant impact on the real-life application of the device [16]. Analysis on the behaviour of elastomeric bearing with rubber cores was conducted by Rahnavard and Thomas numerically, and the researchers remarked that, the damping of bearing increases with the number of rubber core inserted. The study agreed that introduction of rubber core reduces the stiffness of elastomeric bearing [17].

Choi, Nam and Cho observed that strong earthquake often causes large and irreversible deformation in LCRB. To improve the stability of bearing, shape memory alloy (SMA) wire was introduced as vertical bracings at its four vertices. Hedayati Dezfuli and Alam proposed an improvement to the mechanism proposed by Choi, Nam and Cho by arranging the SMA wire bracings diagonally [18][19].

The lateral displacement of LCRB was reduced to 9% maximum strain when the diagonally braced device is subjected to 200% shear strain, compared to 25% maximum strain exhibited by vertically braced device. However, the improvement in energy dissipation capacity was reduced from 38% to 15% by changing vertical bracings to cross bracings [18][19].

Ozkaya et al. developed novel laminated rubber bearing, namely ball rubber bearing (BRB). A hole is prepared at the centre of conventional bearing and filled with steel balls. The proposed mechanism is proven improves the energy dissipation of bearing, as well as its vertical and lateral stiffnesses [20].

Li et al. proposed a novel elastomeric bearing by replacing the reinforcing steel plates with steel mesh, namely steel mesh reinforced elastomeric isolation bearing (SMREIB). When compared to LRB, the vertical stiffness of SMREIB is greater, while the shear stiffness of SMREIB is lower. However, the device can easily roll over and thus able to accommodate

large relative displacement between substructure and superstructure. For this reason, the device possesses better isolation ability compared to LRB [8]. Fig. 1 shows some innovations made to elastomeric bearing.

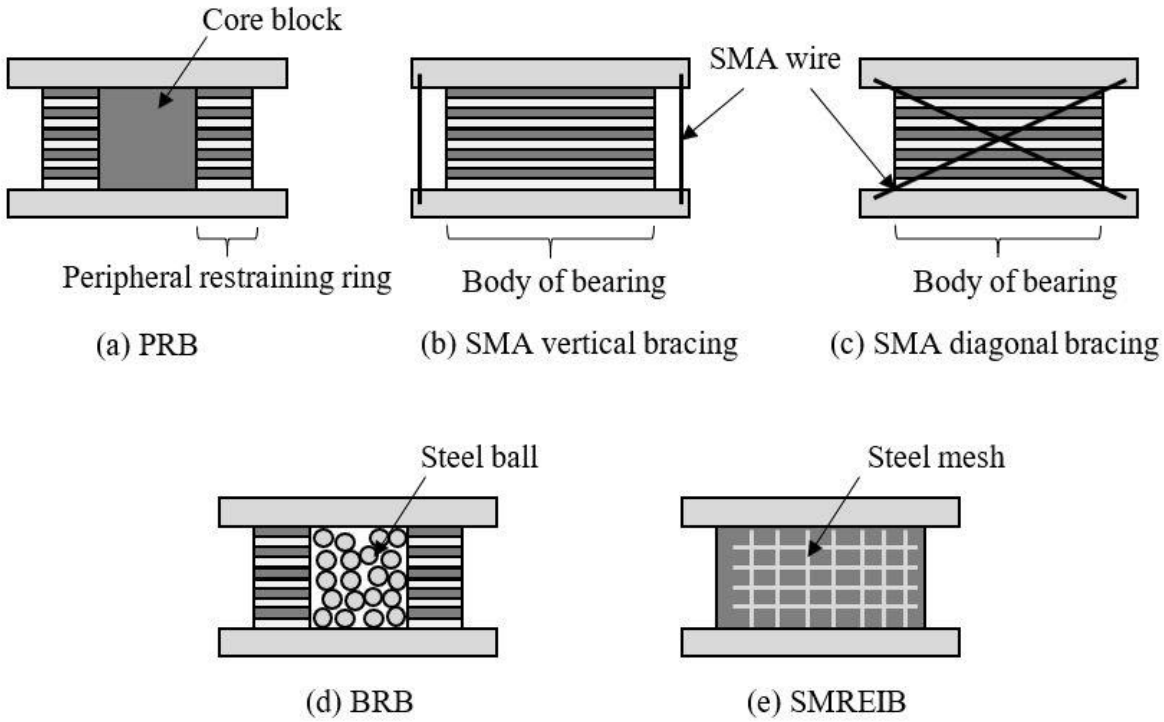

Fig. 1 Innovations and enhancements in bearing technology proposed in previous studies

Among the previously studied improvement on LRB, some deficiencies were identified. For PRB, the introduction of rubber core improved the damping of device by trading off its lateral stiffness [17]. Same situation was observed for SMREIB [8]. The use of sophisticated material such as shape memory alloy requires higher fabrication cost, and this is expected to hinder mass production and wide implementation in future. BRB showed good improvement in both energy dissipation and stiffness, but enhancement can be done by using more common material, which aids in future implementation in industry [20].

Numerical analysis of elastomeric bearing was conducted in various studies. Warn and Weisman conducted numerical analysis of elastomeric strip bearing using FEM. The study found significant difference between FEM and experimental result at the low axial load corresponding to the large lateral displacements. The ineffectiveness of neo-Hookean model in simulating the behaviour of rubber is highlighted in the study. The researchers remarked the model does not take the stiffening of rubber under large shear strain into account [21]. Kalfas, Mitoulis & Katakalos conducted numerical analysis to simulate the behaviour of laminated rubber bearing. From the study, Ogden model is found the accurate to simulate the behaviour of natural rubber [22].

Zhou, Wu and Li studied the behaviour of elastomeric bearing under compression and shear using FEM. The researchers remarked that Mooney-Rivlin model is not able to simulate the behaviour of rubber under stiffening due to huge shear deformation [23].

Modelling of granular material can be conducted in two ways. One of the ways is to model the individual particles using discrete element modelling (DEM) [24]. This method has been implemented in simulation of sand behaviour such as direct shear and triaxial compression tests [25][26]. The main disadvantage of DEM was unusually high computational cost [27][28][29]. The other way is to model the whole sand mass as continuum.

Several types of models were used to simulate the behaviour of granular solids, namely elastic (EL), porous elastic (PE), elastic with Mohr-Coulomb plasticity (ELMC), elastic with Drucker-Prager plasticity (ELDP) and porous elastic with Drucker-Prager plasticity (PEDP) [30].
In the present study, an innovative mechanism for laminated rubber bearings is proposed to improve its performance and implement it in structures and bridges as alternative to lead rubber bearings. The proposed laminated bearings utilized with the steel core and granular and shape memory polymer filler system, and numerical simulation has been conducted to evaluated performance of developed base isolators in comparison to LRB under applied lateral loads.
Also, the prototype of proposed base isolator with two different mentioned fillers are fabricated and experimentally tested under cyclic load to assess the efficacy of developed isolator in terms of energy dissipation capability, shear and compression stiffnesses capacity. Then, the numerical analysis result is validated by using experimental result.

2.0 Development of base isolation utilized with core-and-filler mechanism

In this research work, a rubber base isolator with core-and-filler system is developed as alternative to lead-core rubber bearing (LCRB) which recently considered as extensive environmental contamination due to toxicity impact of lead material. Details of implemented filler systems and core are demonstrated in follow:

2.1 Filler system for base isolation

The function of filler is to improve the bearing's stiffness and damping properties. In this study, two different types of material as granular and shape memory polymers are used as filler materials to improve the efficiency of rubber isolator to dissipate vibrations.
Granular material is proposed as a type of filler for its ability to generate friction when the particles are being pushed by force exerted on bearing. Based on the principle of conservation of energy, such friction plays vital role in dissipating energy which induced by external work done.
Pure sand is used in this study as granular material filler. It is worthy to highlight that gravel mixture is not implemented in this research since previous studies have found that addition of large particles i.e. gravel to sand would not improve the shear strength of mixture significantly [31]. Moreover, large particles impose greater abrasion damage to contacting steel components compared to smaller particles like sand [32]. After collision with steel components, gravel is more prone to be crushed into smaller particles compared to sand, diminishing improvement in mixture's shear strength if there is any [33]. Therefore, pure sand is proposed to use as filler material for base isolation. Application of sand is also beneficial for the industrial implementation of proposed system on elastomeric bearing in future. Sand is a common construction material that involves in concrete mixing, pavement construction, earthwork filling operation etc. By using a material which the construction industries are familiar with, the adaptation of new bearing system can be implemented with less obstacles, compared to the other well-known materials.
Shape memory polymer is another type of filler proposed for the base isolator system. This kind of material is known for its superelasticity and ability to restore back to original shape. Epoxy resin is the kind of shape memory polymer chosen for its wide application in construction industry, such as structural adhesive and pavement engineering [34].
An study shown that material binder treated with epoxy resin became more resilient against rutting compared to the untreated [35]. However, the epoxy resin in use should be flexible enough since the binder treated with high content of epoxy resin became hard and brittle. The strength of such mixture is limited and premature failure often occur before the strength of epoxy is fully deployed [36]. Epoxy with certain degree of flexibility is less likely to show brittle failure [37].

2.2 Steel core system for base isolation

The steel core is used on the developed base isolator for two purposes. Its primary purpose is to improve the strength of filler in resisting shear force that acts laterally. This concept was motivated by an experiment which found that sand becomes stiffer when hard core is inserted in it, compared to those without any core [38]. Its secondary purpose is to limit the bearing from exhibiting large lateral deformation. When the displacement is greater than the allocated horizontal gap, contact or pounding of steel core and bearing body occurs and limit movement to the allowable displacement and prevent of any excessive movement. The core is chamfered at the top to ensure it does not leave any sharp edge that may damage the body of bearing when contact occurs. Gap exists between the top of core and the soffit of bearing top cover plate. This gap is used to prevent the contact between core and top cover plate after the bearing is loaded and compressed. This avoids damages in both components when the bearing is pressed vertically and pushed laterally during operation. The bearing is to be designed in such a way that the gap will still present even when unusually large compression is acting from above. Fig. 2 shows how the bearing responds under different situation.

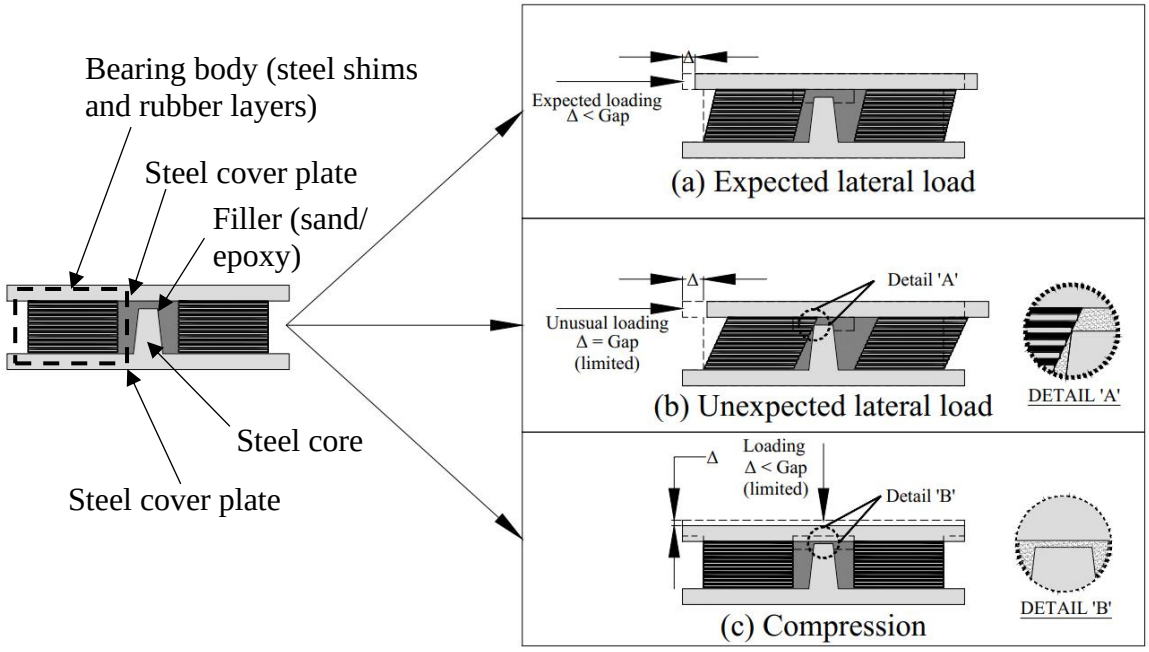

Fig. 2 Bearing response under various loading conditions

3.0 Bearing dimensions

In the present study, the proposed circular elastomeric bearings were consisting of 11 rubber layers and (n_r=11) 10 steel shims (n_s=10). Two rectangular steel plates, namely top and bottom cover plates were used to sandwich the elastomeric bearing. Two types of bearing body were presented in this study. The type 1 body was used in conventional laminated rubber bearing (LRB), while type 2 body was used in sand-core rubber bearing (SCRB) and epoxy-core rubber bearing (ECRB). The key difference between two types of bearing body was the presence of concentric hole at the centre of steel shims and rubber layers in type 2 body. The hole was prepared to accommodate the proposed core-and-filler mechanism inside the elastomeric bearing.

For both types of bearing, the width and length of top and bottom plate were 375mm (W_{top}=W_{bot}=L_{top}=L_{bot}=375mm), while their thickness were 20mm (T_{top}=T_{bot}=20mm). The thickness of steel shims was 3mm (t_s=3mm). The thickness of rubber layers varies with its position, where the two outermost layers ($n_{r,o}$=2) which contacting the cover plates were 4mm ($t_{r,o}$=4mm) and the remaining ($n_{r,i}$=9) were 3mm ($t_{r,i}$=3mm). The diameter of steel shims and rubber layers was 275mm (D_b=275mm). Nominal cover to steel shims was provided, but it was neglected during numerical analysis [39]. The overall height of elastomeric bearing was 65mm (H_b=65mm).

For bearing body type 2, 75mm diameter hole was provided at the centre of all steel shims and rubber layers (D_{void}=75mm). Non-prismatic steel core was provided, where the diameter of core changed from 15mm at the bottom to 10mm at the top ($D_{c,bot}$=15mm, $D_{c,top}$=10mm). The height of core is 35mm (H_{core}=35mm) and therefore, the body of core stem was sloped at a rise to run ratio of 14:1.

In ECRB, the void at the centre of elastomeric bearing was fully filled by epoxy resin (H_{fill}=65mm). In SCRB, two types of filling conditions were established. For the first filling condition, the void was partially filled by silica sand until the height of 35mm, which made the top of filler at the same level with the top of steel core (H_{fill}=35mm). For the second filling condition, the void was fully filled by silica sand (H_{fill}=65mm). The fill volume for ECRB and SCRB2 was approximately 282694mm^3, while that for SCRB1 was approximately 150158mm^3. The centre of bottom cover plate was to be drilled and threaded to fit the steel core, which was threaded at the bottom part. The cover plates were to be manufactured separately, rather than as parts of an integrated unit with elastomeric bearing. This was necessary for the filling process which came later the formation of components. To hold the elastomeric bearing in place between the cover plates during cyclic shear test, restraining rings were provided and welded to both cover plates.

Table 1 summarizes the dimension of all elastomeric bearing models. Fig. 3 shows the schematic drawing of all four elastomeric bearings prepared in the present study.

Table 1 Dimension of elastomeric bearing models

Model ID	Description	Elastomeric bearing					
		Cover plates $W_{top} \times L_{top} \times T_{top}$	Outer rubber layers $D_b \times t_{r,o} \times n_{r,o}$ (D_{void})	Inner rubber layers $D_b \times t_{r,i} \times n_{r,i}$ (D_{void})	Steel shims $D_b \times t_s \times n_s$ (D_{void})	Steel core $D_{c,top}/D_{c,bot} \times H_{core}$	Filler H_{fill}
LRB	Conventional bearing with type 1 bearing body	$375 \times 375 \times 20$	$275 \times 4 \times 2(0)$	$275 \times 3 \times 9(0)$	$275 \times 3 \times 10(0)$	-	-
SCRB1	Type 2 bearing body with void partially filled by coarse silica sand	$375 \times 375 \times 20$	$275 \times 4 \times 2(75)$	$275 \times 3 \times 9(75)$	$275 \times 3 \times 10(75)$	$10/15 \times 35$	35

SCRB2	Type 2 bearing body with void fully filled by coarse silica sand	$375 \times 375 \times 20$	$275 \times 4 \times 2(75)$	$275 \times 3 \times 9(75)$	$275 \times 3 \times 10(75)$	$10/15 \times 35$	65
ECRB	Type 2 bearing body with void fully filled by epoxy resin	$375 \times 375 \times 20$	$275 \times 4 \times 2(75)$	$275 \times 3 \times 9(75)$	$275 \times 3 \times 10(75)$	$10/15 \times 35$	65

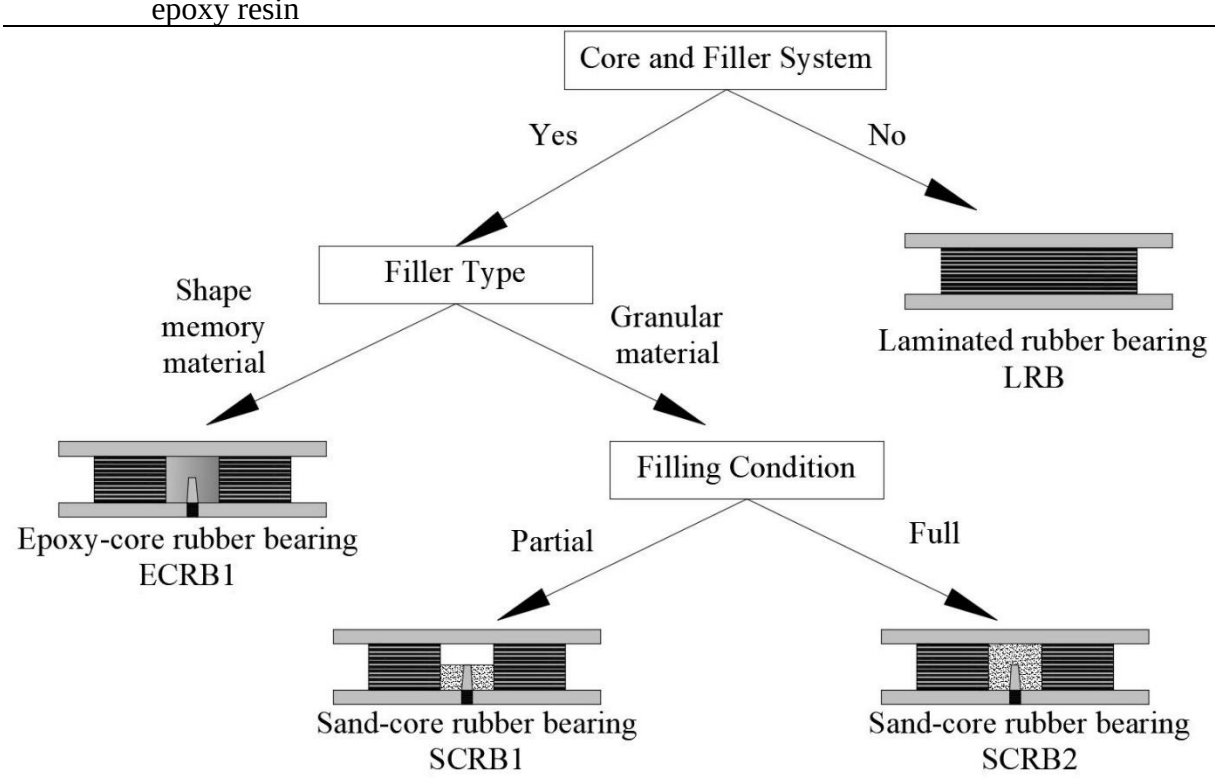

Fig. 3 Elastomeric bearing models prepared in this study

3.1 Filler preparation

The constituent material of the proposed bearing was chloroprene rubber. It was used for its better strength and durability compared to natural rubber. The hardness of rubber proposed was IRHD 60, and the corresponding shear modulus was 0.9±0.15N/mm^2 [40].

For filler, coarse silica sand which sized between 0.63mm to 2mm was used as granular filler [41]. Epoxy resin was used as shape memory polymer filler. It consisted of components A and B. Component A contained an epoxy resin while component B is a hardener. Both components A and B were mixed with weight ratio of 3:1. Based on the information provided by supplier, the composition of shape memory polymer is 65% of oxirane, 2,2' – [(1-methylethylidene) bis (4,1-phenyleneoxymethylene)] bis-, homopolymer, 35% of polyoxy propylenediamine and 10% of benzyl alcohol.

During fabrication stage, the mixture of component A and B was to be stirred thoroughly for 3 minutes before being poured into the void of elastomeric bearing. The elastomeric bearing was clamped together with its bottom cover plate to avoid the outflow from the base of bearing due to irregularity of the surface. The bearing was then left for at least 48 hours for epoxy resin to cure. Fig. 4 shows the condition of bearing prototypes after

(a) SCRB1 (b) SCRB2 (c) ECRB

Fig. 4 Elastomeric bearing prototypes prepared after filling process

4.0 Numerical modelling

Finite element models of proposed elastomeric bearings were developed by using ABAQUS software. The models were simulated and analysis conducted, and the numerical analysis results were exported from the software.

4.1 Material property

This section demonstrates the mechanical properties of all the materials adopted in the simulation of proposed elastomeric bearing using finite element method.

4.1.1 Rubber material

Being the constitutive material used in elastomeric bearing, the definition of mechanical properties of rubber was found crucial during modelling. This section explicitly discusses the properties adopted when defining the rubber material. Through uniaxial test result, for instance the classical experimental result presented by Treloar, linear stress-strain relationship is observed for small strain. In large strain, the relationship becomes non-linear and even so, the elasticity of the material remains. Such behaviour of elastomer is usually defined using hyperelastic model in finite element analysis. Some assumptions are usually made during the analysis. First, the material is considered isotropic, where the same mechanical properties are consistent throughout the continuum, and its behaviour is independent of the location and orientation of loading.

Numerous hyperelastic models are available in ABAQUS [42]. Among them, Ogden model was adopted in this study. The ability of Ogden hyperelastic model in predicting the behaviour of rubber has been found reliable [22]. The strain-energy function W for Ogden hyperelastic model is shown in Eq.(1) [42]:

$$W = \sum_{i=1}^{N} \frac{2\mu_i}{\alpha_i^2}\left[\lambda_1^{\alpha_i} + \lambda_2^{\alpha_i} + \lambda_3^{\alpha_i} - 3\right] \tag{1}$$

Where λ_1, λ_2 and λ_3 are principal stretches. N is the order of strain-energy function, while μ_i and α_i are material constants. In present study, 3rd order function was implemented for all bearing model, with the material constants shown in Table 2 [43].

Table 2 Material constants of Ogden hyperelastic model used for rubber material

	μ	α
1	0.3326	2.4466
2	0.3326	2.4466
3	0.3326	2.4466

μ_0 can be determined based on the Ogden hyperelastic model material constants by using Eq. (2) [42]. In present study, the calculated μ_0 was 0.9978MPa, which was consistent with the specification for rubber material. The Mullins effect was neglected for simplicity, as suggested by Altalabani et al. [44].

$$\mu_0 = \sum_{i=1}^{N} \mu_i = 0.9978MPa \tag{2}$$

The initial bulk modulus K_0 and initial shear modulus μ_0 were taken as 2000MPa and 0.9978MPa respectively [40]. The Poisson's ratio, v can be determined using Eq. given the values of K_0 and μ_0 [42].

$$v = \frac{3\,K_0/\mu_0 - 2}{6\,K_0/\mu_0 + 2} = \frac{3(2000/0.9978) - 2}{6(2000/0.9978) + 2} = 0.4998 \tag{3}$$

Given high K_0/μ_0 ratio of rubber which leads to high v, the compressibility is insignificant compared to shear flexibility. Therefore, it is suitable to consider rubber an incompressible material.

The damping behaviour of rubber material can be simulated by implementing hysteresis parameters. These parameters were introduced by Bergstrom and Boyce, which consists of stress scaling factor S, creep parameter $\hat{C}_1$, effective stress exponent m and creep strain exponent C_2 [45]. S is the tested stress ratio under instantaneous loading which affects the damping ratio of elastomer. Effective creep strain is described by $\hat{C}_1$. m describes the dependency of effective stress to creep strain rate [17]. C_2 was defined as -1 by Bergstrom and Boyce, however ABAQUS allowed it to be defined as a value ranging between -1 to 0 [45][42]. In present study, cyclic shear test produced hysteresis curve, and this made the implementation of hysteresis parameters necessary. Bergstrom and Boyce suggested a set of hysteresis parameters which may be applicable to common elastomer. However, modification of these parameters was recommended by the researchers to fit the model to experimental result [45]. Trial-and-error were conducted on LRB model in present study to determine an appropriate set of hysteresis parameters, as per the method implemented by Khaloo, Barmi and Moeini [46]. The parameters presented by Bergstrom and Boyce for chloroprene rubber with 15% of carbon black N600 by volume was used as first trial, where the value of S is obtained by calculating the ratio of μ_B to μ_A, which were 4.45MPa and 1.31MPa respectively [47]. They were implemented to LRB at first, and trial-and-error was conducted until a suitable hysteresis curve that fit the experimental results was produced. The resultant parameters were then implemented to all elastomeric bearings for numerical simulation. The set of parameters obtained from this process is presented in Table 3.

Table 3 Hysteresis parameters defined for rubber material

Stress scaling factor S	Creep parameter $\hat{C}_1$	Effective stress exponent m	Creep strain exponent C_2
50	4×10^{-10}	8	0

4.1.2 Steel material

The behaviour of steel was described as elastoplastic in finite element analysis. The modulus of elasticity E and Poisson's ratio v of steel were taken as 210GPa and 0.3, respectively [48]. The yield strength σ_y of steel material is taken as 235MPa [40]. However, yielding of the steel components was not anticipated throughout the simulation (Refer to Table 4).

4.1.3 Sand material

Sand presented in SCRB1 and SCRB2. To simulate the behaviour of sand, finite element method was used rather than discrete element method. The computation cost for discrete element method is high and the implementation was deemed impractical [29].

By using finite element method, the sand filler was modelled as an entire sand mass as a result. The behaviour of sand was described as linear elastic [30], where the modulus of elasticity E and Poisson's ratio v were taken as 85MPa and 0.3 respectively [49][50] (Refer to Table 4).

4.1.4 Epoxy material

Epoxy presented in ECRB. Its behaviour governed by elastoplastic during finite element analysis. The mechanical properties of epoxy resin were based on the value reported in literature. Modulus of elasticity E and Poisson's ratio v of epoxy resin were taken as 1038MPa and 0.35, respectively [51]. Its yield stress σ_y was taken as 15.8MPa and the corresponding yield strain ε_y was 1.07%. The epoxy material was expected to fail at ultimate stress σ_{max} of 26.5MPa, with the corresponding elongation at break ε_{max} of 2.9% [52].

4.1.5 Lead material

Lead-core rubber bearing was simulated in finite element analysis, and its performance was used as the benchmark to evaluate the performance of elastomeric bearing with proposed core-and-filler system. The behaviour is lead was defined as elastoplastic. The elastic properties, namely modulus of elasticity E and Poisson's ratio v were 18GPa and 0.43, respectively [44]. The yield strength of lead was taken as 10MPa [7].

Table 4 summarizes the mechanical properties adopted for steel, sand, epoxy and lead materials in finite element analysis.

Table 4 Mechanical properties of steel, sand, epoxy and lead

Material	Model	Properties
Steel	General elasticity [48]	E=210GPa
		v=0.3
	General plasticity [40]	σ_y=235MPa
Sand	General elasticity [49][50]	E=85MPa
		v=0.3
Epoxy	General elasticity [51]	E=1038MPa
		v=0.35
	General plasticity [52]	σ_y=15.8MPa
		ε_y=1.07%
		σ_y=26.5MPa
		ε_y=2.9%
Lead	General elasticity [44]	E=18GPa
		v=0.43
	General plasticity [7]	σ_y=10MPa

4.2 Model meshing

Hex shape element was used to mesh all components in elastomeric bearing models. C3D8R element, namely reduced integration linear hexahedral solid element with eight-node and three degree of freedom under hourglass control was used to model steel shims, steel core, top and bottom plate, epoxy and lead. On the other hand, C3D8RH element, namely reduced integration linear hexahedral solid element with eight-node and three degree of freedom under hourglass control and hybrid with constant pressure was implemented for rubber layers. Linear triangular

prism with six-node and three degree of freedom (C3D6) element was implemented for sand mass.

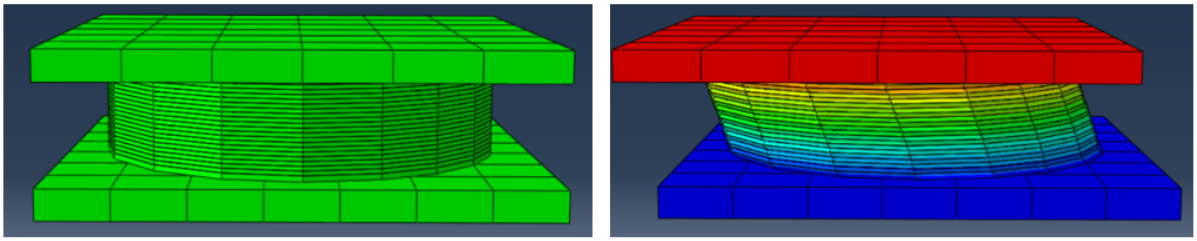

(a) Unloaded condition (b) Deformation during cyclic shear test

Fig. 5 Proposed elastomeric bearing during finite element simulation

4.3 Loading and interaction

Both benchmark LRB and proposed elastomeric bearings were tested in accordance with the requirement stated by AASHTO. Article 13.3 of the AASHTO guideline was referred when planning for the test programme [53]. Three fully reversed cycles of shear were applied on the bearing alongside with compression. In present study, the design compression was 180kN and the total design displacement *TDD* was set as 30mm.

The design axial load was applied to the centre of top face of top cover plate as concentrated load. All nodes on the top face were connected to the loading point via beam type multi-point constraint, which is available in ABAQUS [42]. Design lateral displacement of 30mm was applied as cyclic lateral displacement at the loading point. Three sinusoidal cycles of horizontal displacement were defined and applied laterally, with the frequency of 0.0566Hz, or 0.349rad/s in circular frequency (Fig. 6).

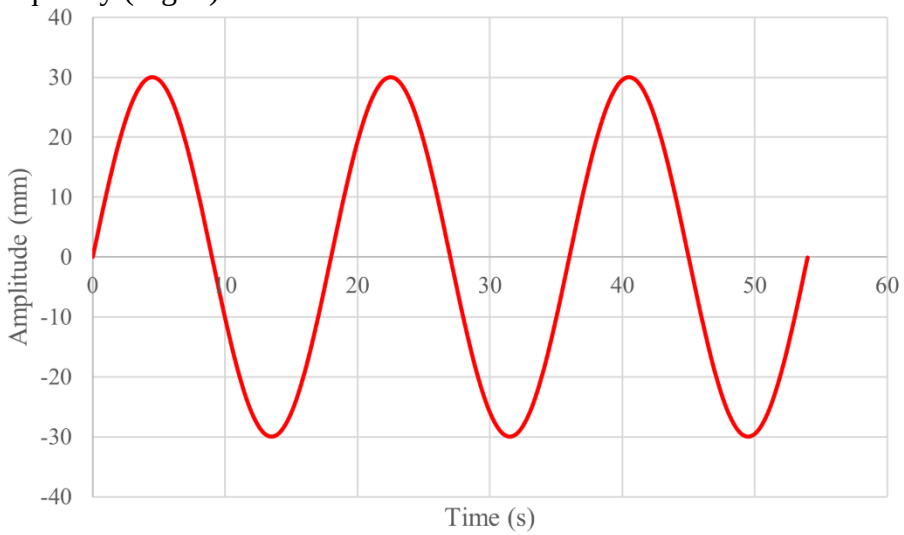

Fig. 6 Sinusoidal lateral displacement cycles applied during finite element simulation

The axial load was exerted in the first step of analysis while the cyclic lateral displacement was applied in the second step. The axial load was propagated to the second step, simulating the combination of axial load and lateral displacement during cyclic shear test.

The soffit of bottom cover plate was defined as encastre, where the displacement and rotation of all nodes locating on this face were not allowed. This boundary condition was established prior to the analysis.

The bond between steel shims and rubber layers was usually formed through vulcanization. This process involved heat and pressure, and eventually formed the elastomeric bearing as a single unit. This adhesion was defined using tie constraint [54]. The core was expected to stay intact throughout the test. Therefore, the connection between bottom cover plate and steel core was established using tie constraint. Tie constraints was established for the contact interface between cover plates and outer rubber layers as well, given the ability of restraining ring to hold the bearing in place.

For ECRB, adhesion between elastomeric bearing components and the epoxy formed. For SCRB1 and SCRB2, the tangential contact can be modelled as rough where no slippage of the contacting surfaces is allowed [55]. Moreover, contact in normal direction was expected to be hard where no penetration was allowed. The sand mass was expected to move together with the elastomeric bearing and stay in contact with the bearing components. Therefore, no separation between sand mass and bearing body was considered. Based on these justifications, the contact between elastomeric bearing components and filler was established using tie constraint, which simplified the contact behaviour above and optimized the analysis runtime. Tie constraint was used to describe the interaction between lead core and contacting elastomeric bearing components as well [44].

4.4 Simulation results

Characteristics of an isolation system are usually described using effective stiffness k_{eff}, damping ratio ξ, characteristics strength Q and post-yield stiffness, k_d. These parameters were derived from the lateral force-displacement curve obtained through cyclic shear test. The calculation methods for these characteristics are presented in Eqs.(4), (5), (6) and (7) [44][8]:

$$k_{eff} = \frac{F_p - F_n}{d_p - d_n} \tag{4}$$

$$\xi = \frac{2EDC}{\pi k_{eff}\left(d_p - d_n\right)^2} \tag{5}$$

$$Q = \frac{1}{2}\left(Q_p - Q_n\right) \tag{6}$$

$$k_d = \frac{1}{2}\left(\frac{F_p - Q_p}{d_p} - \frac{F_n - Q_n}{d_n}\right) \tag{7}$$

Where d_p and d_n are the maximum positive and negative displacement applied throughout the test. F_p and F_n are the force corresponding to d_p and d_n, respectively. *EDC* is the total energy dissipated in every cycle, which is determined by measuring the hysteresis loop area from lateral force-displacement curve. Q_p and Q_n are the positive and negative intersection of the curve and vertical axis. Fig. 7 shows the graphical definition of the parameters and characteristics that can be determined from a lateral force-displacement curve.

In present study, the third loop of the cyclic shear test result was used to determine the characteristics of elastomeric bearings.

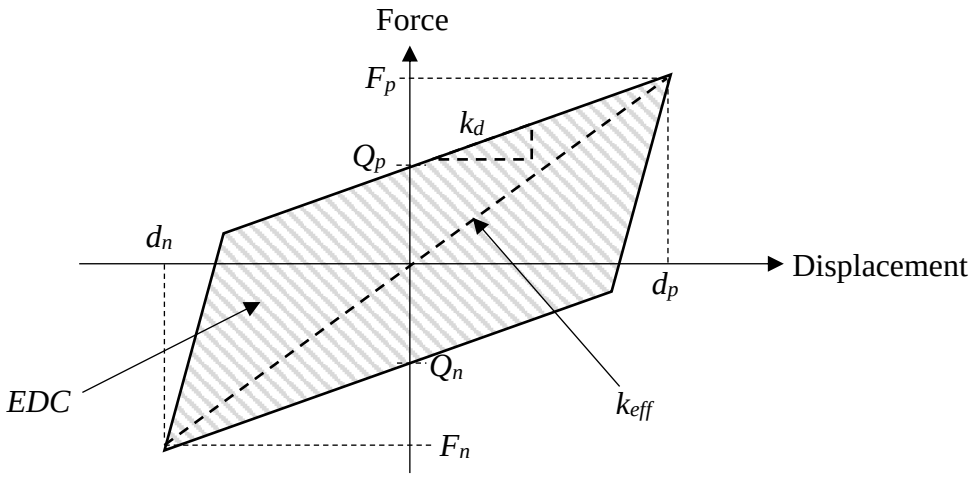

Fig. 7 Parameters and characteristics of elastomeric bearing in lateral force-displacement curve

Based on finite element analysis, the improvement in terms of k_{eff} was shown for all bearings with core-and-filler system when compared to LRB. Among them, the improvement was the greatest for SCRB2 i.e. 32.0% and the smallest for SCRB1 i.e. 3.2%. In terms of *EDC*, the performance of bearing weakened when sand filler wis used, as seen from the reduction of 7.8% and 12.1% for SCRB1 and SCRB2 respectively. Conversely, by using epoxy the *EDC* is predicted to improve by 9.1%. ξ decreased for all proposed bearing by different degree, from the -10.6% for SCRB1 to -33.4% for SCRB2. Simulation predicted decrement of Q for bearing with sand filler, and improvement for epoxy filler. Negative k_d value was predicted for LRB, indicating the reduction in resistance of elastomeric bearing with increasing stroke was anticipated.

When compared to LCRB, bearings with full filler height showed improvement in terms of k_{eff}, with the greatest improvement of 15.4% by SCRB2. Partially filled bearing on the other hand, did not prove itself to be a good alternative to LCRB in terms of stiffness. Nonetheless, replacement of lead core with full sand brought deterioration in *EDC* by 2.4%, while others showed improvement by 2.4% and 21.1% for SCRB1 and ECRB respectively. Similar trend was identified for ξ, where both SCRB1 and ECRB led to improvement of 13.6% and 6.8%, while SCRB2 brought reduction of ξ by 15.3%. LCRB possessed higher Q compared to bearings with sand filler, but not for epoxy. The characteristics of elastomeric bearings based on numerical analysis result is shown in Table 5.

Table 5 Characteristics of elastomeric bearings from finite element analysis results

Model	LRB	LCRB	SCRB1	SCRB2	ECRB
d_p (mm)	30	30	30	30	30
d_n (mm)	-30	-30	-30	-30	-30
F_p (kN)	393.5	452.2	405.2	522.5	509.7
F_n (kN)	-381	-434.4	-393.8	-499.7	-495.3
Q_p (kN)	418.5	401.2	391.2	379	454.1
Q_n (kN)	-418.3	-401.7	-390.7	-380.6	-453.7
EDC (kNmm)	41105.3	37026	37895.6	36143.1	44841
k_{eff} (kN/mm)	12.91	14.78	13.32	17.05	16.76
ξ *(%)*	56.34	44.33	50.35	37.55	47.36
Q (kN)	418.4	401.5	390.9	379.8	453.9
k_d (kN/mm)	-1.04	1.40	0.29	4.38	1.62

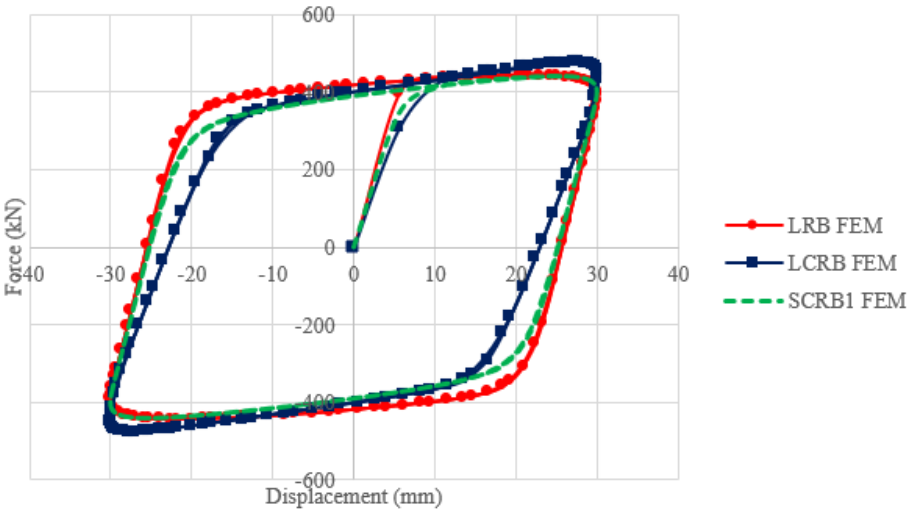

(a) SCRB1, LRB and LCRB

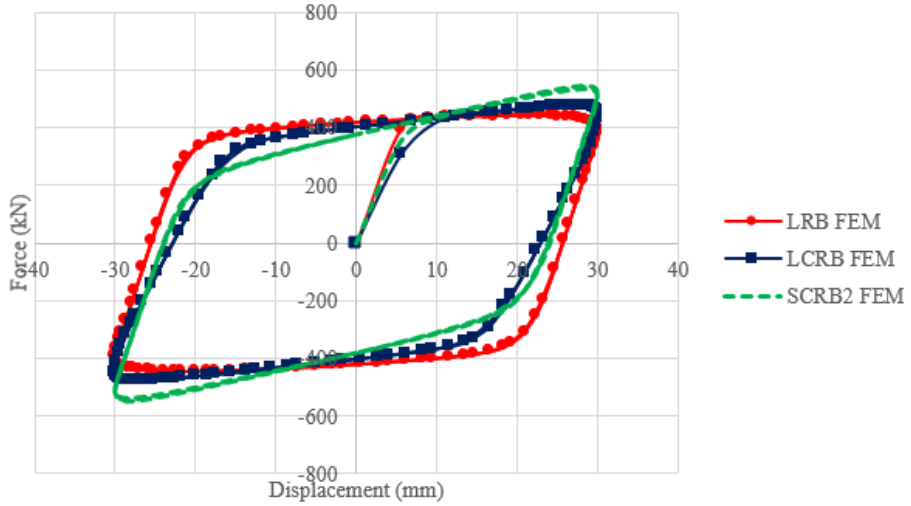

(b) SCRB2, LRB and LCRB

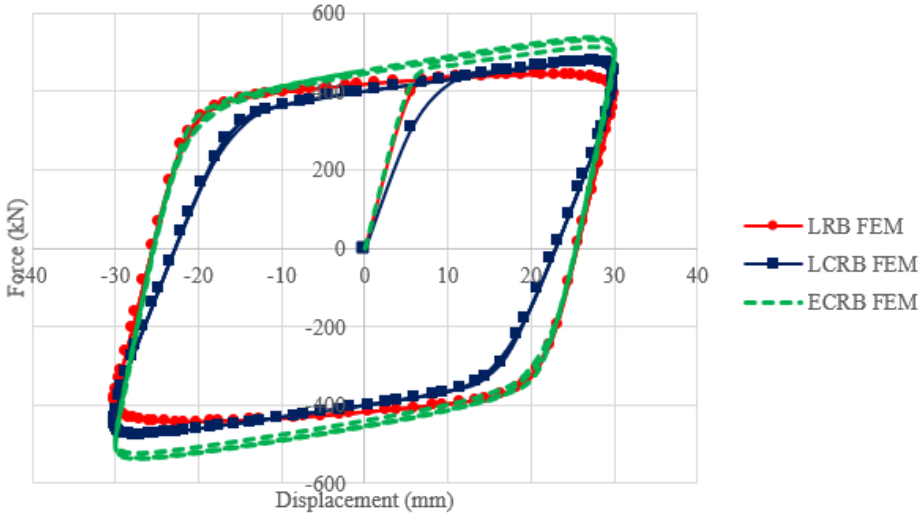

(c) ECRB, LRB and LCRB

Fig. 8 Comparison of hysteresis loop obtained from finite element analysis for elastomeric bearings

5.0 Experiment

Experiment was conducted based on the loading conditions simulated during finite element simulation. Three model prototypes were manufactured and tested, and the experimental results were extracted and analysed.

5.1 Experimental setup

The top and bottom cover plates of bearing were welded to two different loading plates which dimension fits in the testing machine. Four 45mm diameter steel rods were placed on the top of loading plate and served as roller. Two steel cuboids were welded to two opposite edges of top loading plate to retain the roller and prevent them from dropping out of the loading plate during the test. The function of roller was to ensure the top of tested bearing is free to move along the direction of applied displacement while being compressed. The rolling resistance to the stroke due to roller was negligible. Three dynamic actuators were used, where one of them was tasked to applied compression of 180kN on the elastomeric bearings and two of them were tasked to stroke the top loading plate by 30mm back and forth. Fig. 9 shows the setup for experiment, while Fig. 10 demonstrates the loading mechanism for the conducted test.

A linear variable differential transformer (LVDT) was used to measure the lateral displacement of top loading plate. The loading rate for bearings was 0.0556Hz or 6.7mm/s. In relation to that, the test duration for bearings was 54s. Refer to Fig. 11 for the bearing condition during throughout the test.

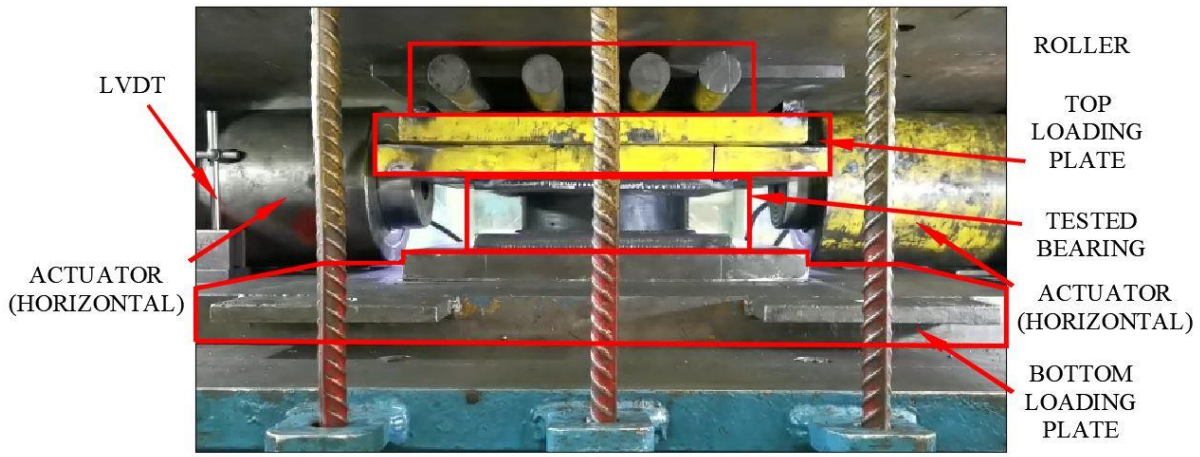

Fig. 9 Test setup for cyclic shear test

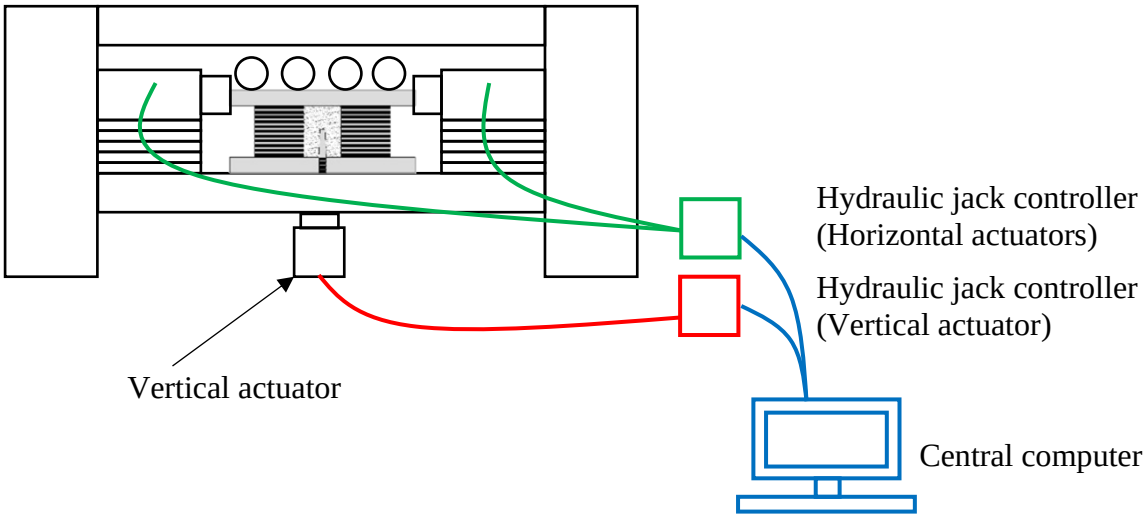

(1) Pre-test condition

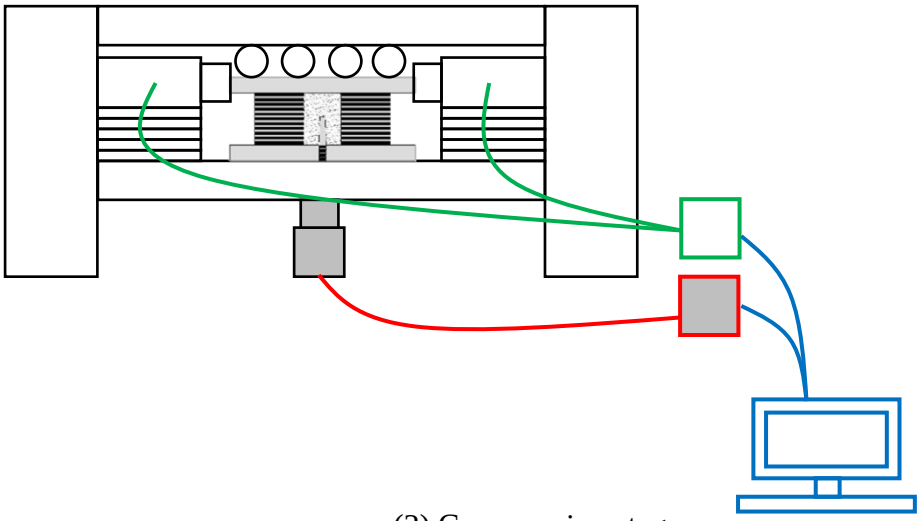

(2) Compression stage

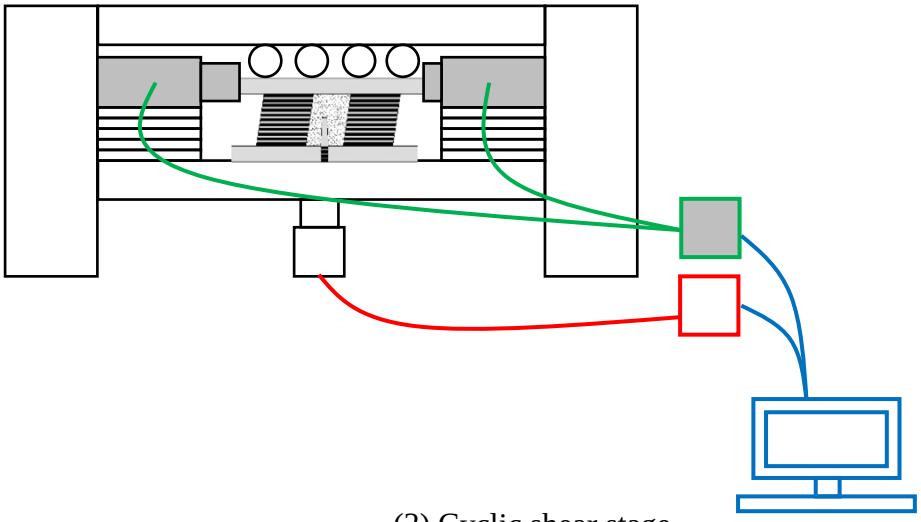

(3) Cyclic shear stage

Fig. 10 Loading mechanism for cyclic shear test

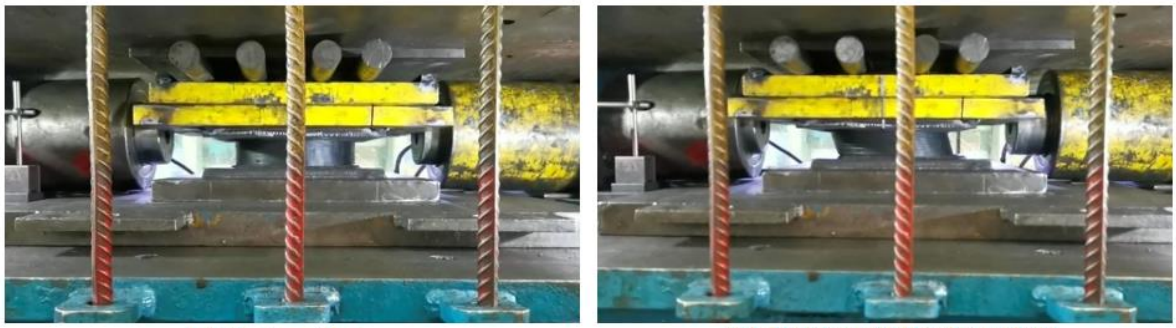

(a) Before test (b) During cyclic shear test

Fig. 11 Condition of elastomeric bearing

5.2 Experimental results

The bearing characteristics were determined using Eqs.(4), (5), (6) and (7). Generally, the stiffness k_{eff}, characteristics strength Q and post-yield stiffness k_d of LRB improved when core-and-filler system was introduced. When comparing the performance of all proposed elastomeric bearings with benchmark LRB, SCRB2 was found giving the greatest improvement among on elastomeric bearing stiffness. Its improvements in k_{eff} and Q were 21.5% and 24.2% respectively. On the other hand, ECRB showed least improvement for k_{eff} at 5.9%, but with intermediate level of improvements for Q when compared with SCRB1 and SCRB2, which was 7.7% respectively. The improvement in k_d is the most significant comparing to all the bearing characteristics. Such improvement ranging from 37% for SCRB1 to 57.7% for SCRB2. The damping ratio ξ for LRB decreases when core-and-filler system was introduced, by up to 5.9% as seen in SCRB1. The result from experiment is shown in Table 6. Fig. 12 shows the lateral force-displacement curve from experiment.

Table 6 Characteristics of elastomeric bearings from experimental results

Model	LRB	SCRB1	SCRB2	ECRB
d_p (mm)	31	31.9	32.4	32.1
d_n (mm)	-30.9	-31.5	-32.9	-32.9
F_p (kN)	410	450	529	459
F_n (kN)	-418	-452	-532	-462
Q_p (kN)	350	376	444	386
Q_n (kN)	-399	-415	-486	-421
EDC (kNmm)	41917.15	44009.45	54838.8	47921.1
k_{eff} (kN/mm)	13.376	14.227	16.248	14.169
ξ *(%)*	52.06	48.99	50.38	50.95
Q (kN)	374.5	395.5	465	403.5
k_d (kN/mm)	1.28	1.75	2.01	1.76

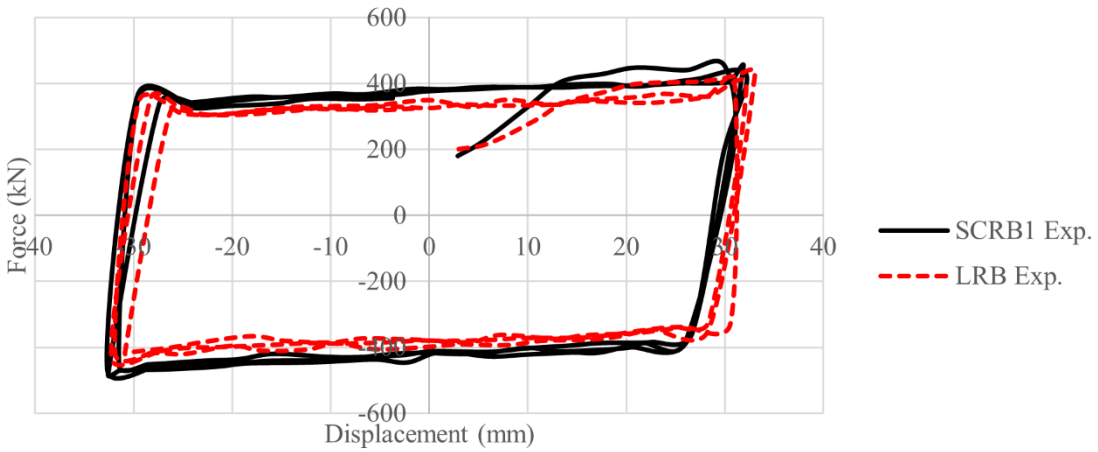

(a) SCRB1 and LRB

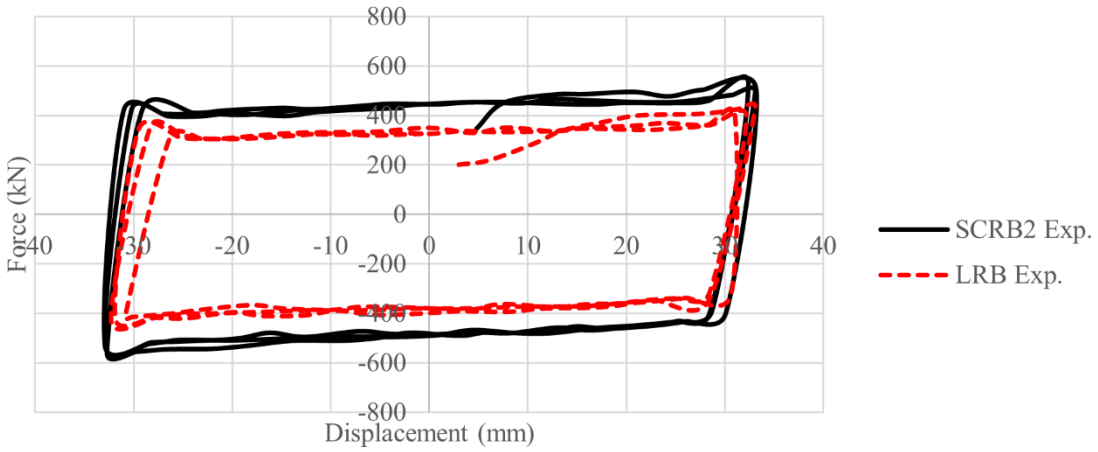

(b) SCRB2 and LRB

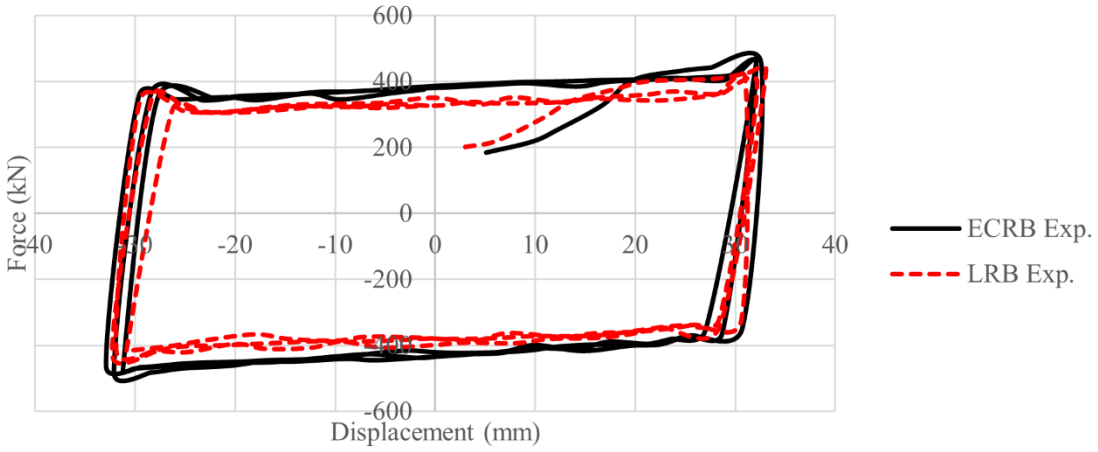

(c) ECRB and LRB

Fig. 12 Hysteresis loop obtained from experiment for elastomeric bearings

The purpose of validation of finite element models was to determine if the numerical analysis agrees with the physical concept. Therefore, this process is essential to assess the reliability of numerical simulation. In present study, the finite element analysis results were validated by comparing the output with the experimental results presented in previous section. The lateral force-displacement curves from both experiment and numerical analysis were qualitatively

compared and inspected. Then, deviation from elastomeric bearing characteristics extracted from both sets of results was calculated.

In general, finite element analysis underestimates the *EDC* of all elastomeric bearings equipped with proposed core-and-filler mechanism. Among these bearings, the deviation of ECRB was the lowest (Δ=-6.4%). The deviation for SCRB1 and SCRB2 were -13.9% and -34.1% respectively. On the other hand, *EDC* for LRB obtained from numerical analysis was in good agreement with the experimental result.

k_{eff} was underestimated for both LRB (Δ=-3.5%) and SCRB1 (Δ=-6.4%), and overestimated for both SCRB2 (Δ=+4.9%) and ECRB (Δ=+18.3%). ξ derived from the *EDC* and k_{eff} obtained from finite element analysis was found greater than those from bearing test result for LRB (Δ=+8.2%) and SCRB1 (Δ=+2.8%). Contrary, the value of ξ calculated based on the outcome from numerical analysis was lower than experimental result for SCRB2 (Δ=-25.5%) and ECRB (Δ=-7.0%). *Q* derived from finite element analysis was found greater than that from experiment for LRB (Δ=+11.7%) and ECRB (Δ=+12.5%). The value is less than the actual result for SCRB1 (Δ=-1.2%) and SCRB2 (Δ=-18.3%).

The error in k_d between the results from experiment and numerical analysis was found the greatest for LRB, SCRB1 and SCRB2, where the deviation was -181.5%, -83.7% and +117.9% respectively. Such deviation was relatively insignificant for ECRB (Δ=-7.8%).

Table 7 presents the error between the experimental result and finite element analysis result for all experimentally tested bearings. Fig. 13 shows the comparison of output from finite element analysis with experimental results.

Table 7 Comparison of the elastomeric bearings' characteristics from experiment and numerical analysis

	Model	LRB	SCRB1	SCRB2	ECRB
EDC(kNmm)	Exp.	41917.15	44009.45	54838.8	47921.1
	FEM	41105.3	37895.6	36143.1	44841
	Δ (%)	-1.9	-13.9	-34.1	-6.4
k_{eff} (kN/mm)	Exp.	13.376	14.227	16.248	14.169
	FEM	12.91	13.32	17.05	16.76
	Δ (%)	-3.5	-6.4	+4.9	+18.3
ξ (%)	Exp.	52.06	48.99	50.38	50.95
	FEM	56.34	50.35	37.55	47.36
	Δ (%)	+8.2	+2.8	-25.5	-7.0
Q (kN)	Exp.	374.5	395.5	465	403.5
	FEM	418.4	390.9	379.8	453.9
	Δ (%)	+11.7	-1.2	-18.3	+12.5
k_d (kN/mm)	Exp.	1.28	1.75	2.01	1.76
	FEM	-1.04	0.29	4.38	1.62
	Δ (%)	-181.5	-83.7	+117.9	-7.8

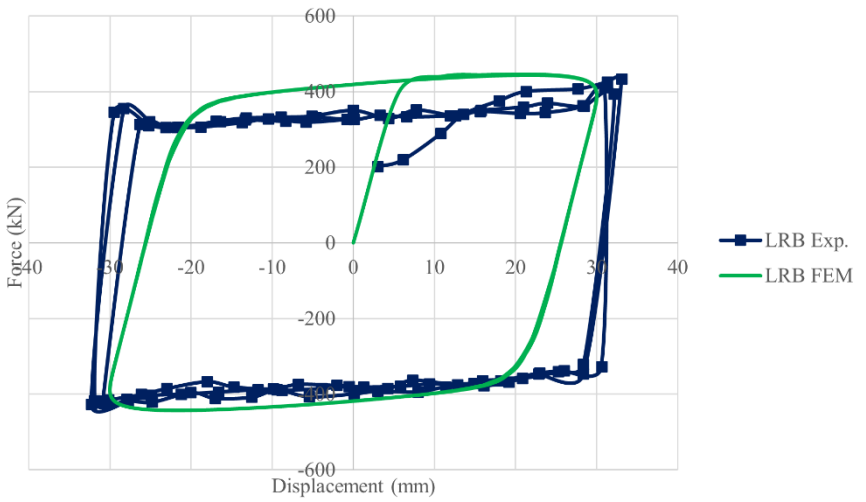

(a) LRB

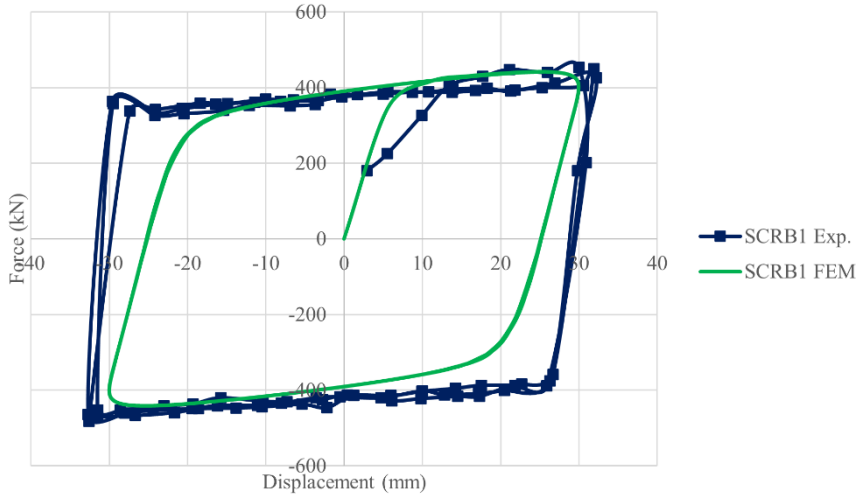

(b) SCRB1

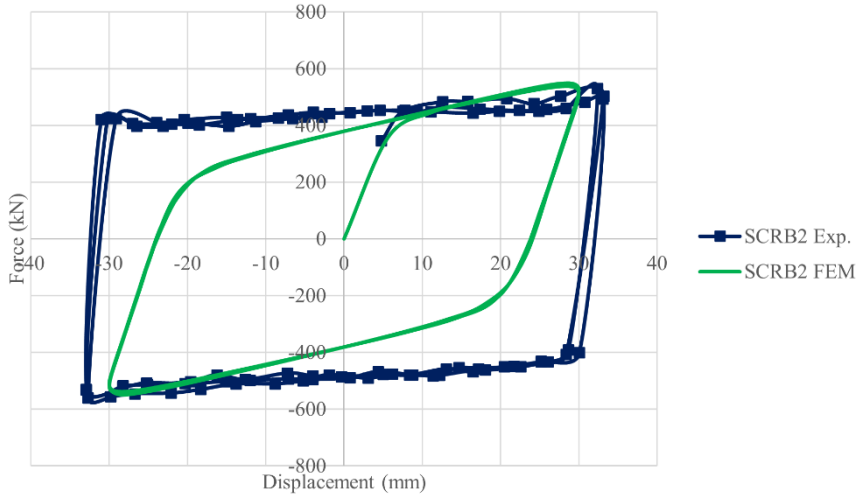

(c) SCRB2

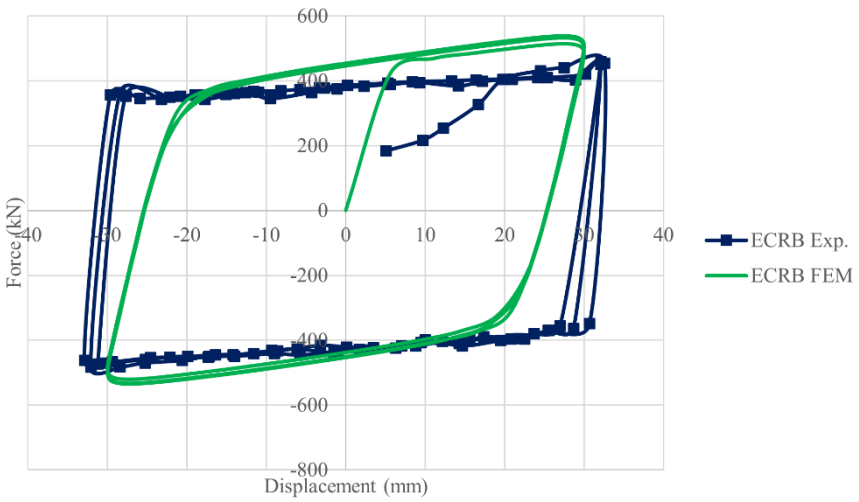

(d) ECRB

Fig. 13 Comparison of hysteresis curve obtained from experiment and numerical analysis for elastomeric bearings

6.0 Discussions

The proposed core-and-filler mechanism improves the strength and energy dissipation of elastomeric bearings. When the superstructure on bearing is moving laterally, the inner face of elastomeric bearing pushes the filler and activates its function.

When the void is partially filled by coarse sand, k_{eff} improves by 6.4% while the *EDC* improves by 5.0%. The characteristics strength *Q* improves by 5.6% on the other hand. This shows the improvement in energy dissipation is inferior to the improvement in terms of strength. In SCRB1, since the sand is free from confining pressure, the shear strength of sand is negligible. When subjected to lateral force, the counteracting friction developed between interlocking sand particles is insignificant since the sand particle will choose to move elsewhere and experiences minimal interparticle friction. Nonetheless, this is only applicable to the sand particles near to the top level of filler. For particles located at mid-depth and bottom of the mass, they are considered confined by the self weight of sand mass above. Such confinement may not be significant, but it is sufficient to lead to a situation where the interparticle friction increases with depth of filler. Moreover, the confined part of sand mass can effectively transfer the stress to steel core and activates its shear resistance.

SCRB2 exhibits improvements as much as 30.8% for *EDC*, 21.5% for k_{eff} and 24.2% for *Q*. Under fully filled condition, the sand mass is confined by elastomeric bearing body and cover plates. When loaded axially, the pressure is transferred to sand mass through top cover plate. As a result, the shear strength of sand mass is greater with the presence of confining pressure, compared to the partially filled condition in SCRB1. In other words, the contribution of sand mass to shear strength of elastomeric bearing is more significant than SCRB1. On top of that, the resistance of steel core is fully activated over the full height of sand-steel core contact interface, since the sand particles do not move around and always remain in contact with the steel core entirely.

The difference between SCRB2 and SCRB1 is the presence of sand mass above the top level of steel core. This additional sand mass contributes to shear strength using solely interparticle friction. It is believed that with the presence of this sand mass, the *EDC* greatly improves and makes the improvement more superior than that for strength. Therefore, it can be concluded that steel core mainly contributes to the improvement of bearing strength and stiffness, while being governed by the sand-steel core contact interface. The shear strength of sand, which is dependent of the exerted normal stress, does not appear to be a significant contributor to overall

stiffness of bearing. On the other hand, sand mass contributes to energy dissipation via its internal damping. As seen from SCRB1, the height of sand mass is the same as the height of core, and the improvements in strength (k_{eff} and Q) and energy dissipation are consistent, ranging from 5.00% to 6.36%.

In ECRB, the improvement in *EDC* is superior to that in k_{eff}. When compared to SCRB1 and SCRB2, it shows epoxy provides less stiffness to elastomeric bearing, and this shows epoxy has higher flexibility compared to coarse sand mass. On the other hand, while showing similar degree of improvement in terms of stiffness with SCRB1, the improvement in *EDC* is more obvious for ECRB. This is benefit from the superelasticity and shape memory property of epoxy.

Core-and-filler system greatly improve the post yield stiffness k_d of elastomeric bearing. Bearing with high k_d value exhibits small residual drift, which proves the system efficient in controlling the displacement of bearing and superstructure. The value of k_d is almost the same for both SCRB1 and ECRB. Moreover, k_d for SCRB2 is about 14.3% greater than that for ECRB. This shows coarse sand filler is more effective in controlling the residual drift, where its half-filled condition is equivalent to the performance of epoxy under fully-filled condition.

Through the cyclic shear test, LRB has higher damping ratio ξ compared to all bearings with core-and-filler system. Rubber is proven superior in providing the damping ratio for elastomeric bearing compared to sand and epoxy. The isolation effect detriments with the improvement in stiffness, as observed from the increase in k_{eff} often accompanied by decrease in ξ. For LRB, total plan area of rubber is 59395.7mm^2, while that for bearings with core-and-filler system is 54978mm^2, which is around 7.4% less than that for LRB. As a result, the reduction in damping ratio for SCRB1, SCRB2 and ECRB are 5.9%, 3.2% and 2.2% respectively. While the trade-off is inevitable, it shows SCRB2 performs better and more efficient than other bearings, with an improvement of 21.5% in terms of k_{eff}, while having only 3.2% of reduction in ξ.

Among three types of core-and-filler system, epoxy filler possesses highest damping ratio (50.95%), where the reduction from LRB is 2.2%. From this perspective, the epoxy filler-and-core system is more suitable for seismic isolation purpose. However, post-test condition of ECRB is inspected and damage can be observed on the top of filler (Fig. 14). Thus, epoxy filler is subjected to deterioration over time and the performance of elastomeric bearing is expected to drop over time. On the other hand, sand mass which consists of granulates is not susceptible to damage under compression and shear. The granulates are too stiff to deform, yet free enough to move along with the elastomeric bearing.

When bearing is compressed, the stress applied to sand mass and make it tightly packed. When lateral displacement is applied, the movement reshuffles the arrangement of granulates. The compaction-reshuffle cycle grants sand mass restoring ability that enables it to perform consistently over long time. Moreover, the ability is only activated when needed e.g. upon the movement, and this minimize the frequency of abrasion between granulates and with other bearing components. Knowing the grinding and crushing of granulates and abrasion on the steel and rubber component may deteriorate the performance of bearing, by reducing the unnecessary movement and abrasion, the service life span of elastomeric bearing can be prolonged.

The maintenance of core-and-filler system is either the replacement of filler or steel core. To conduct either replacement for a system with epoxy filler, effort is required to remove the hardened epoxy. Moreover, the bearing is not fit for duty immediately after maintenance as the curing of epoxy takes time. When sand filler is used, the maintenance is more convenient and require less effort than using epoxy as filler. In the event of steel core replacement, the original sand filler can be reused.

Fig. 14 Damage observed on the top of epoxy filler

Hyperelastic and hysteresis properties of rubber obtained from trial and error is adequate. This can be seen from small deviation for both k_{eff} and *EDC* when comparing the results for LRB obtained from finite element analysis with experiment.
However, imperfection is observed from the hysteresis model proposed by Bergstrom & Boyce in describing the rubber material in tested elastomeric bearing. As opposed to experimental results, the magnitude of Q_p is greater than F_p, and the same trait is observed for F_n and Q_n. As a result, negative k_d value is obtained for LRB. Due to the overestimated Q_p and Q_n, the value of Q for LRB is overestimated. Such inaccuracy of finite element analysis may due to the mechanical properties of chloroprene rubber, where its unloading behaviour is less time dependent [56]. As a result, the predicted hysteresis curve shows good agreement during loading stage, but relatively poor agreement during unloading stage, as shown in Fig. 15.

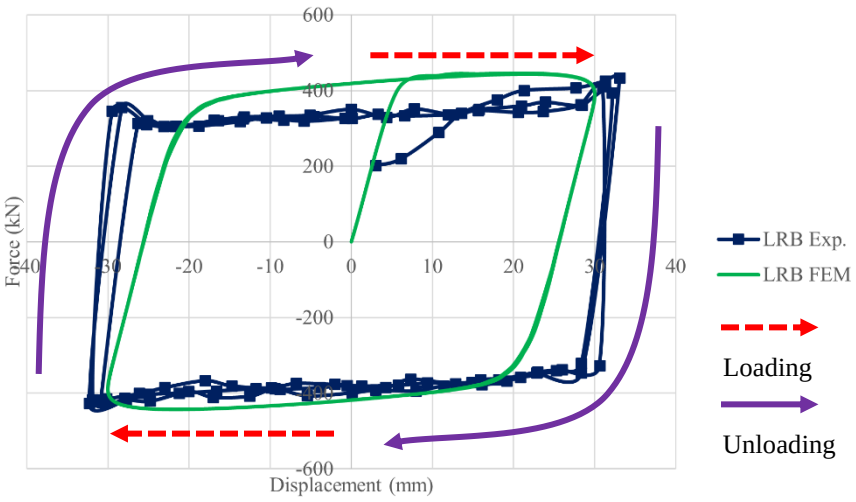

Fig. 15 Hysteresis behaviour for LRB in the view of loading and unloading stages

Elastoplastic model for epoxy is suitable as seen from small deviation in terms of *EDC*. The stiffness and characteristics strength of ECRB is overestimated, indicating the actual material

is weaker than the properties defined during finite element analysis. The deviation between k_d is negligible and there is no sign of negative stiffness value as observed from LRB. This is due to the definition of epoxy simply as an elastoplastic material, where the material improves the strength of ECRB without worsen the imperfection in hysteresis material model, comparing to LRB. The definition of sand as elastic model, alongside tie constraint is suitable in producing satisfying finite element analysis result. By considering only elastic properties of sand, the strength of elastomeric bearing can be described properly, which can be observed from deviations in terms of k_{eff} for both SCRB1 and SCRB2. The adequacy is better when compared to epoxy, where the deviation in terms of k_{eff} is greater. Nonetheless, by neglecting the plasticity behaviour of sand, the numerical analysis will not take the hardening of stressed sand into account, and this leads to significant underestimation in terms of *EDC*. This can be seen from the resultant hysteresis curves shown in Fig. 8, where the hysteresis curve is almost identical for all cycles, as opposed to ECRB where noticeable difference for each cycle presents, denoting the effect of plasticity definition in epoxy material.

This effect is more obvious when large amount of sand is modelled, as seen from SCRB2. Similar as ECRB, the numerical analysis yields positive k_d value for both SCRB1 and SCRB2, although the accuracy is poor compared to ECRB. k_d for SCRB1 is nearly zero, indicating small effect from the replacement of rubber with pure elastic sand in producing correct bearing's hysteresis behaviour that produces proper k_d value. On the other hand, there is too much of such effect in SCRB2 that ends up with hugely overestimated k_d.

Based on the result obtained, the improvement of accuracy in terms of any of two commonly used elastomeric bearing characteristics i.e. k_{eff} and *EDC*, often require trade-off from the other. On the other hand, by the definition of ξ, its deviation comes from the amplification of error from k_{eff} and *EDC*. Nonetheless, the shape of hysteresis curves produced by finite element models were showing good agreement with that from experimental results, given the accurate loading stage prediction that yields fairly accurate k_{eff}, which is one of the most important parameters that used to idealise the stiffness component of elastomeric bearing during structural analysis [57].

7.0 Conclusions

In the present study, an attempt has been made to develop an innovative laminated rubber bearing base isolator by utilizing the steel core and granular and shape memory polymer filler system. For granular filler, silica sand was used, and two types of filling condition viz partially and fully filled were considered to evaluate the performance. However, for shape memory polymer, epoxy resin was fully filled in the core-and-filler system.

The finite element model was developed for the proposed elastomeric bearings to simulate their behaviour under the testing condition. Thereafter, based on numerical analysis results, prototype of developed LRB isolators manufactured and its performance experimentally tested by applying cyclic load and the outcome was compared with the benchmark LRB for comparison purpose. Then, the analysis models were validated using experimental results to determine their reliability in predicting the behaviour of bearings.

From the conducted finite element analysis and experimental test, the following findings are drawn and summarized:

1. Finite element analysis proves the replacement of lead with full height filler brings improvement in effective stiffness, i.e. 15.3% and 13.4% for SCRB2 and ECRB. Use of epoxy also showed improvement in energy dissipation by 21.1%.
2. The proposed core-and-filler system can be introduced as an effective high performance LRB device, as seen from the improvement in terms of bearing performance with the minimum of 6.4% and 5.0% for effective stiffness and energy dissipation capacity, respectively. This may lead to more economical bearing design.

3. The shear stiffness of elastomeric bearing with fully height sand and steel core is superior to all tested elastomeric bearings. The improvement in shear stiffness by 21.5% is significant while the drawback in the form of reduction in damping ratio by 3.2% is small, when the fully height sand was implemented in LRB.
4. Epoxy filler is susceptible to irreversible damage when operate in long term. On the other hand, sand filler is anticipated to perform consistently as the granules are too stiff to deform and the entire sand mass possesses restoring ability whenever it is subjected to combined compression and shear.
5. Rubber is superior in providing damping for elastomeric bearing, in comparing to sand and epoxy with steel core. This can be seen from the reduction in terms of bearing damping ratio after proposed core-and-filler system is introduced. The damping ratios are 48.99%, 50.38% and 50.95% for SCRB1, SCRB2 and ECRB respectively, in opposed to 52.06% for benchmark LRB.
6. Replacement of lead core with fully filled granular and shape memory filler improves the shear stiffness of bearing. Improvement of 15.4% and 13.4% is achieved by SCRB2 and ECRB respectively. This proves the device is more effective in limiting the displacement of elastomeric bearing when it is subjected to lateral load.
7. Imperfection is identified in the hysteresis model when describing the behaviour of rubber in the tested elastomeric bearings. This is seen from the overestimation of Q_p and Q_n, and the underestimation of F_p and F_n for LRB which yields negative post yield stiffness. This is due to the time-independent properties of chloroprene rubber during unloading, which is not accurately simulated during finite element analysis. As a result, for bearing where its stiffness is heavily relies on the rubber i.e. LRB, the post yield stiffness is -1.04kN/mm. On the other hand, the issue is not seen for bearings that are not heavily rely on the rubber to gain stiffness, where the post yield stiffness calculated is 0.29kN/mm, 4.38kN/mm and 1.62kN/mm for SCRB1, SCRB2 and ECRB respectively.
8. Linear elastic model and tie constraint with other elastomeric bearing components is suitable in predicting the behaviour of sand in the proposed core-and-filler system.

Declaration of Competing Interest

The authors declare that they have no known competing financial interests or personal relationships that could have appeared to influence the work reported in this paper.

References

[1] Clemente P, Bongiovanni G, Buffarini G, Saitta F, Castellano MG, Scafati F. Effectiveness of HDRB isolation systems under low energy earthquakes. Soil Dynamics and Earthquake Engineering 2019; 118: 207–220. https://doi.org/10.1016/j.soildyn.2018.12.018.

[2] Burtscher SL, Dorfmann A. Compression and shear tests of anisotropic high damping rubber bearings. Engineering Structures 2004; 26(13): 1979–1991. https://doi.org/10.1016/j.engstruct.2004.07.014.

[3] Markou AA, Manolis GD. Mechanical models for shear behavior in high damping rubber bearings. Soil Dynamics and Earthquake Engineering 2016; 90: 221–226. http://doi.org/10.1016/j.soildyn.2016.08.035.

[4] Marano GC, Greco R. Effciency of base isolation systems in structural seismic protection and energetic assessment. Earthquake Engineering & Structural Dynamics 2003; 32(10): 1505-1531, 2003. https://doi.org/10.1002/eqe.286.

[5] Cardone D, Gesualdi G, Nigro D. Effects of air temperature on the cyclic behavior of elastomeric seismic isolators. Bulletin of Earthquake Engineering 2011; 9(4): 1227–1255. https://doi.org/10.1007/s10518-011-9244-8.
[6] Chaudhary MTA, Abé M, Fujino Y. Performance evaluation of base-isolated Yama-agé bridge with high damping rubber bearings using recorded seismic data. Engineering Structures 2001; 23(8): 902–910. https://doi.org/10.1016/S0141-0296(00)00117-6.
[7] Robinson WH. Lead-rubber hysteretic bearings suitable for protecting structures during earthquakes. Earthquake Engineering & Structural Dynamics 1982; 10(4): 593–604. https://doi.org/10.1002/eqe.4290100408.
[8] Li H, Tian S, Dang X, Yuan W, Wei K. Performance of steel mesh reinforced elastomeric isolation bearing: Experimental study. Construction and Building Materials 2016; 121: 60–68. http://doi.org/10.1016/j.conbuildmat.2016.05.143.
[9] Kang BS, Li L, Ku TW. Dynamic response characteristics of seismic isolation systems for building structures. Journal of Mechanical Science and Technology 2009; 23(8): 2179–2192. https://doi.org/10.1007/s12206-009-0437-x.
[10] Jangid RS, Kelly JM. Base isolation for near-fault motions. Earthquake Engineering & Structural Dynamics 2001; 30(5): 691-707. https://doi.org/10.1002/eqe.31.
[11] Kim SH, Mha HS, Lee SW. Effects of bearing damage upon seismic behaviors of a multi-span girder bridge. Engineering Structures 2006; 28(7): 1071–1080. https://doi.org/10.1016/j.engstruct.2005.11.015.
[12] Gottesfield P, Were FH, Adogame L, Gharbi S, San D, Nota MM, Kuepouo G. Soil contamination from lead battery manufacturing and recycling in seven African countries. Environmental Research 2018; 161: 609–614 https://doi.org/10.1016/j.envres.2017.11.055.
[13] Gałuszka A, Migaszewski ZM, Dołęgowska S, Michalik A. Geochemical anomalies of trace elements in unremediated soils of Mt. Karczówka, a historic lead mining area in the city of Kielce, Poland. Science of Total Environment 2018; 639: 397–405. https://doi.org/10.1016/j.scitotenv.2018.05.174.
[14] Bose-O'Reilly S, Yabe J, Makumba J, Schutzmeier P, Ericson B, Caravanos J. Lead intoxicated children in Kabwe, Zambia. Environmental Research 2018; 165: 420–424. https://doi.org/10.1016/j.envres.2017.10.024.
[15] Clay K, Portnykh M, Severnini E. The legacy lead deposition in soils and its impact on cognitive function in preschool-aged children in the United States. Economics & Human Biology 2019; 33: 181-192. https://doi.org/10.1016/j.ehb.2019.03.001.
[16] Matsushita H, Fujisawa K, Sasaki T. Development of peripherally restraining type seismic isolator. SMiRT-12 1993; K25/4: 375-380.
[17] Rahnavard R, Thomas RJ. Numerical evaluation of steel-rubber isolator with single and multiple rubber cores. Engineering Structures 2019; 198: 109532. https://doi.org/10.1016/j.engstruct.2019.109532.
[18] Choi E, Nam T, Cho BS. A new concept of isolation bearings for highway steel bridges using shape memory alloys. Canadian Journal of Civil Engineering 2005; 32(5): 957–967. https://doi.org/10.1139/l05-049.
[19] Hedayati Dezfuli F, Alam M S. Performance-based assessment and design of FRP-based high damping rubber bearing incorporated with shape memory alloy wires. Engineering Structures 2014; 61: 166–183. https://doi.org/10.1016/j.engstruct.2014.01.008.
[20] Ozkaya C, Akyuz U, Caner A, Dicleli M, Pinarbasi S. Development of a new rubber seismic isolator: 'Ball Rubber Bearing (BRB)'. Earthquake Engineering & Structural Dynamics 2011; 40(12): 1337-1352. https://doi.org/10.1002/eqe.1091.

[21] Warn GP, Weisman J. Parametric finite element investigation of the critical load capacity of elastomeric strip bearings. Engineering Structures 2011; 33(12): 3509–3515. http://doi.org/10.1016/j.engstruct.2011.07.013.
[22] Kalfas KN, Mitoulis SA, Katakalos K. Numerical study on the response of steel-laminated elastomeric bearings subjected to variable axial loads and development of local tensile stresses. Engineering Structures 2017; 134: 346–357. http://doi.org/10.1016/j.engstruct.2016.12.015.
[23] Zhou T, Wu YF, Li AQ. Numerical study on the ultimate behavior of elastomeric bearings under combined compression and shear. KSCE Journal of Civil Engineering 2018; 22(9): 3556–3566. https://doi.org/10.1007/s12205-018-0949-y.
[24] Cundall PA, Strack ODL. The discrete numerical model for granular assemblies. Geotechnique 1979; 29(1): 47-65. https://doi.org/10.1680/geot.1979.29.1.47.
[25] Belheine N, Plassiard JP, Donze FV, Darve F, Seridi A. Numerical simulation of drained triaxial test using 3D discrete element modelling. Computers and Geotechnics 2009; 36(1-2): 320-331. https://doi.org/10.1016/j.compgeo.2008.02.003.
[26] Yan Y, Ji S. Discrete element modeling of direct shear tests for a granular material. International Journal for Numerical and Analytical Methods in Geomechanics 2010; 34(9): 978-990. https://doi.org/10.1002/nag.848.
[27] Lim KW, Andrade JE. Granular element method for three-dimensional discrete element calculations. International Journal for Numerical and Analytical Methods in Geomechanics 2014; 38(2): 167-188. https://doi.org/10.1002/nag.2203.
[28] Kawamoto R, Ando E, Viggiani G, Andrade JE. Level set discrete element method for three-dimensional computations with triaxial case study. Journal of the Mechanics and Physics of Solids 2016; 91: 1-13. https://doi.org/10.1016/j.jmps.2016.02.021.
[29] Tong L, Wang YH. DEM simulations of shear modulus and damping ratio of sand with emphasis on the effects of particle number, particle shape, and aging. Acta Geotechnica 2015; 10: 117-130. https://doi.org/10.1007/s11440-014-0331-2.
[30] Ai J, Chen JF, Ooi JY. Finite element simulation of the pressure dip in sandpiles. International Journal of Solids and Structures 2013; 50: 981-995. https://dx.doi.org/10.1016/j.ijsolstr.2012.12.006.
[31] Chang WJ, Phantachang T. Effects of gravel content on shear resistance of gravelly soils. Engineering Geology 2016; 207: 78-90. http://doi.org/10.1016/j.enggeo.2016.04.015.
[32] Wei Y, Yang Y, Tao M. Effects of gravel content and particle size on abrasivity of sandy gravel mixture. Engineering Geology 2018; 243: 26-35. https://doi.org/10.1016/j.enggeo.2018.06.009.
[33] Weibull W. A statistical distribution function of wide applicablility. Journal of Applied Mechanics 1951; 18: 293-297.
[34] Zhang K, Wang L, Wang F, Wang G, Li Z. Preparation and characterization of modified-clay-reinforced and toughened epoxy-resin nanocomposites. Journal of Applied Polymer Science 2004; 91: 2649-2652. https://doi.org/10.1002/app.13445.
[35] Kang Y, Song M, Pu L, Liu T. Rheological behaviors of epoxy asphalt binder in comparison of base asphalt binder and SBS modified asphalt binder. Construction and Building Materials 2015; 76: 343-350. https://dx.doi.org/10.1016/j.conbuildmat.2014.12.020.
[36] Zhang Q, Xu YH, Wen ZG. Influence of water-borne epoxy resin content on performance of waterborne epoxy resin compound SBR modified emulsified asphalt for tack coat. Construction and Building Materials 2017; 153: 774-782. https://doi.org/10.1016/j.conbuildmat.2017.07.148.

[37] Voo R, Mariatti M, Sim LC. Flexibility improvement of epoxy nanocomposites thin films using various flexibilizing additives. Composites: Part B 2012; 43: 3037-3043. http://dx.doi.org/10.1016/j.compositesb.2012.05.032.
[38] Mohapatra SR, Rajagopal K, Sharma J. Direct shear tests on geosynthetic-encased granular columns. Geotextiles and Geomembranes 2016; 44: 396-405. http://dx.doi.org/10.1016/j.geotexmem.2016.01.002.
[39] Ohsaki M, Miyamura T, Kohiyama M, Yamashita T, Yamamoto M, Nakamura N. Finite-element analysis of laminated rubber bearing of building frame under seismic excitation. Earthquake Engineering and Structural Dynamics 2015; 44(11): 1881–1898. https://doi.org/10.1002/eqe.2570.
[40] EN 1337-3. Structural bearings Part 3: elastomeric bearings. Brussels: European Committee for Standardization 2005.
[41] ISO. ISO 14688-1 Geotechnical investigation and testing - Identification and classification of soil - Part 1: Identification and description. Geneva: International Organization for Standardization 2002.
[42] ABAQUS®. Theory manual. 2014 Version 6.14.
[43] Wang Y, Liu J, Duan W, Pan Z, Qiao Y. Fatigue of vulcanized natural rubber under proportional and non-proportional loading. Fatigue & Fracture of Engineering Materials & Structures 2020; 43: 2232-2246. https://doi.org/10.1111/ffe.13250.
[44] Altalabani D, Hejazi F, Raizal Saifulnaz MR, Farah Nora Aznieta AA. Development of new rectangular rubber isolators for a tunnel-form structure subjected to seismic excitations. Structures 2021; 32: 1522-1542. https://doi.org/10.1016/j.istruc.2021.03.106.
[45] Bergstrom JS, Boyce MC. Constitutive modeling of the large strain time-dependent behavior of elastomers. Journal of the Mechanics and Physics of Solids 1998; 46: 931-954.
[46] Khaloo A, Barmi AM, Moeini ME. Numerical parametric investigation of hysteretic behavior of steelreinforced elastomeric bearings under large shear deformation. Structures 2020; 26: 456-470. https://doi.org/10.1016/j.istruc.2020.04.029.
[47] Bergstrom JS, Boyce MC. Constitutive modeling of the time-dependent and cyclic loading of elastomers and application to soft biological tissues. Mechanis of Materials 2001; 33: 523-530.
[48] EN 1993-1-1. Eurocode 3: Design of steel structures – Part 1-1: General rules and rules for buildings. Brussels: European Committee for Standardization 2005.
[49] Kamal ZA, Arab MG, Dif A. Analysis of the arching phenomenon of bored piles in sand. Alexandria Engineering Journal 2016; 55: 2639-2645. https://dx.doi.org/10.1016/j.aej.2016.06.035.
[50] Faizi K, Armaghani DJ, Sohaei H, Rashid ASA, Nazir R. Deformation model of sand around short piles under pullout test. Measurement 2015; 63: 110-119. http://dx.doi.org/10.1016/j.measurement.2014.11.028.
[51] Li J, Tian C, Lu B, Xian Y, Wu R, Hu G, Xia R. Deformation behavior of nanoporous gold based composite in compression: A finite element analysis. Composite Structures 2019; 211: 229-235. https://doi.org/10.1016/j.compstruct.2018.12.046.
[52] Hu J, Chen W, Fan P, Gao J, Fang G, Cao Z, Peng F. Epoxy shape memory polymer (SMP): Material preparation, uniaxial tensile tests and dynamic mechanical analysis. Polymer Testing 2017; 62: 335-341. http://dx.doi.org/10.1016/j.polymertesting.2017.07.001.
[53] AASHTO. Guide specifications for seismic isolation design. 4th edition. Washington D.C.: American Association of State Highway and Transportation Officials 2014.

[54] Ren X, Lu W, Zhu Y, He Y, Li T. Compressive behavior of low shape factor lead-rubber bearings: Full-scale testing and numerical modeling. Engineering Structures 2020; 209. https://doi.org/10.1016/j.engstruct.2019.110030.
[55] Potts DM, Dounias GT, Vaughan PR. Finite element analysis of the direct shear box test. Geotechnique 1987; 37 (1): 11-23.
[56] Tang, S., Greene, M.S., Liu, W.K. Two-scale mechanism-based theory of nonlinear viscoelasticity. Journal of the Mechanics and Physics of Solids 2012: 60: 199-226. https://doi.org/10.1016/j.jmps.2011.11.003
[57] Jiang, Y., Zhao, Z., Zhang, R., Domenico, D.D., Pan, C. Optimal design based on analytical solution for storage tank with inerter isolation system. Soil Dynamics and Earthquake Engineering 2020; 129. https://doi.org/10.1016/j.soildyn.2019.105924